

# 1 HIBRID: Histology and ct-DNA based Risk- 2 stratification with Deep Learning

3  
4 Chiara M.L. Loeffler\* (1, 2, 3), Hideaki Bando\* (4,5,6), Srividhya Sainath (1),  
5 Hannah Sophie Muti (1, 2, 7), Xiaofeng Jiang (1), Marko van Treeck (1), Nic Gabriel Reitsam  
6 (1,8,9), Zunamys I. Carrero (1), Tomomi Nishikawa (4), Toshihiro Misumi (4), Saori Mishima  
7 (5), Daisuke Kotani (5), Hiroya Taniguchi (10), Ichiro Takemasa (11), Takeshi Kato (12), Eiji  
8 Oki (13), Tanwei Yuan (14), Durgesh Wankhede (14), Sebastian Foersch (15), Hermann  
9 Brenner (14, 16), Michael Hoffmeister (14), Yoshiaki Nakamura (5,6), Takayuki Yoshino\*  
10 (4,5,6), Jakob Nikolas Kather\* (1, 2, 3, 16)

11

12 \* Equal contribution

13 + Correspondence to [jakob-nikolas.kather@alumni.dkfz.de](mailto:jakob-nikolas.kather@alumni.dkfz.de) and [tyoshino@east.ncc.go.jp](mailto:tyoshino@east.ncc.go.jp)

- 14 1. Else Kroener Fresenius Center for Digital Health, Technical University Dresden,  
15 Dresden, Germany
- 16 2. Medical Department 1, University Hospital and Faculty of Medicine Carl Gustav  
17 Carus, Technische Universität Dresden, Dresden, Germany
- 18 3. National Center for Tumor Diseases Dresden (NCT/UCC), a partnership between  
19 DKFZ, Faculty of Medicine and University Hospital Carl Gustav Carus, TUD Dresden  
20 University of Technology, and Helmholtz-Zentrum Dresden - Rossendorf (HZDR),  
21 Dresden, Germany
- 22 4. Department of Data Science, National Cancer Center Hospital East, Kashiwa, Japan
- 23 5. Department of Gastroenterology and Gastrointestinal Oncology, National Cancer  
24 Center Hospital East, Kashiwa, Japan
- 25 6. Translational Research Support Office, National Cancer Center Hospital East,  
26 Kashiwa, Japan
- 27 7. Department for Visceral, Thoracic and Vascular Surgery, University Hospital and  
28 Faculty of Medicine Carl Gustav Carus, Technische Universität Dresden, Dresden,  
29 Germany
- 30 8. Pathology, Faculty of Medicine, University of Augsburg, Augsburg, Germany
- 31 9. Bavarian Cancer Research Center (BZKF), Augsburg, Germany
- 32 10. Department of Clinical Oncology, Aichi Cancer Center Hospital, Nagoya, Japan
- 33 11. Department of Surgery, Surgical Oncology and Science, Sapporo Medical University,  
34 Sapporo, Japan
- 35 12. Department of Surgery, NHO Osaka National Hospital, Osaka, Japan

36 13. Department of Surgery and Science, Graduate School of Medical Sciences, Kyushu  
37 University, Fukuoka, Japan

38 14. Division of Clinical Epidemiology and Aging Research, German Cancer Research  
39 Center (DKFZ), Heidelberg, Germany

40 15. Institute of Pathology, University Medical Center Mainz, Mainz, Germany.

41 16. Medical Oncology, National Center for Tumor Diseases (NCT), University Hospital  
42 Heidelberg, Heidelberg, Germany

## 43 Highlights

- 44 - This study combines MRD status measured by ctDNA with a DL-based risk  
45 assessment trained on histological image data to enhance recurrence prediction.
- 46 - DL-based spatial assessment of tumor histopathology slides significantly improves  
47 the risk stratification provided by MRD alone.
- 48 - MRD-negative patients with high DL-based risk had a significantly longer DFS if  
49 treated with ACT, compared to MRD-negative and DL low risk patients
- 50 - The DL model is fully open-source and publicly available.

## 51 Keywords

52 Deep Learning, molecular residual disease, circulating tumor DNA, colorectal cancer, vision  
53 transformers

## 54 Abstract

55 **Background:** Although surgical resection is the standard therapy for stage II/III colorectal  
56 cancer (CRC), recurrence rates exceed 30%. Circulating tumor DNA (ctDNA) emerged as a  
57 promising recurrence predictor, detecting molecular residual disease (MRD). However,  
58 spatial information about the tumor and its microenvironment is not directly measured by  
59 ctDNA. Deep Learning (DL) can predict prognosis directly from routine histopathology slides.

60 **Methods:** We developed a DL pipeline utilizing vision transformers to predict disease-free  
61 survival (DFS) based on histological hematoxylin & eosin (H&E) stained whole slide images  
62 (WSIs) from patients with resectable stage II-IV CRC. This model was trained on the DACHS  
63 cohort (n=1766) and independently validated on the GALAXY cohort (n=1555). Patients  
64 were categorized into high- or low-risk groups based on the DL-prediction scores. In the  
65 GALAXY cohort, the DL-scores were combined with the four-weeks post-surgery MRD  
66 status measured by ctDNA for prognostic stratification.

67 **Results:** In GALAXY, the DL-model categorized 307 patients as DL high-risk and 1248  
68 patients as DL low-risk ( $p < 0.001$ ; HR 2.60, CI 95% 2.11-3.21). Combining the DL scores  
69 with the MRD status significantly stratified both the MRD-positive group into DL high-risk  
70 ( $n=81$ ) and DL low-risk ( $n=160$ ) (HR 1.58 (CI 95% 1.17-2.11;  $p=0.002$ ) and the MRD-  
71 negative group into DL high-risk ( $n=226$ ) and DL low-risk ( $n=1088$ ) (HR 2.37 CI 95% 1.73-  
72 3.23;  $p < 0.001$ ). Moreover, MRD-negative patients had significantly longer DFS when  
73 predicted as DL high-risk and treated with ACT (HR 0.48, CI 95% 0.27-0.86;  $p=0.01$ ),  
74 compared to the MRD-negative patients predicted as DL low-risk (HR=1.14, CI 95% 0.8-  
75 1.63;  $p=0.48$ ).

76 **Conclusion:** DL-based spatial assessment of tumor histopathology slides significantly  
77 improves the risk stratification provided by MRD alone. Combining histologic information with  
78 ctDNA yields the most powerful predictor for disease recurrence to date, with the potential to  
79 improve follow-up, withhold adjuvant chemotherapy in low-risk patients and escalate  
80 adjuvant chemotherapy in high-risk patients.

81

## 82 Introduction

83 Colorectal cancer (CRC) is one of the leading causes of cancer-related deaths worldwide<sup>1</sup>.  
84 Surgical resection remains the standard curative therapy in patients with Stage II-III CRC  
85 and resectable metastases. Despite advancements in surgical and adjuvant therapies,  
86 recurrence rates exceed 30% and 60%<sup>2,3</sup>, respectively. Patients who relapse have an  
87 increased mortality risk, hence identifying these patients at an early stage is crucial for  
88 optimising follow-up treatment decisions. Current prognostication systems for risk  
89 assessment, including imaging techniques, clinicopathological features and molecular data,  
90 are moderate predictors for recurrence risk. Similarly, follow-up strategies, such as tumor  
91 marker monitoring with carcinoembryonic antigen (CEA), lack sensitivity and specificity in  
92 identifying recurrence<sup>4-6</sup>. In particular for stage II CRC, the decision on adjuvant  
93 chemotherapy (ACT) is based on diverging risk assessment recommendations provided  
94 through international oncological associations<sup>7,8</sup>. Thus, a more fine-grained system for  
95 estimating the risk of relapse is required, as no stage-specific survival benefit for adjuvant  
96 chemotherapy has been proven. Therefore, new biomarkers for better and more precise  
97 prognostication are needed. Circulating tumor DNA (ctDNA) has emerged as a promising  
98 minimally invasive biomarker that measures a small fraction of ctDNA in the blood, allowing  
99 for the detection of molecular residual disease (MRD) status<sup>9</sup>. Additionally, ctDNA can be  
100 used for monitoring treatment response and early prediction of recurrence, as ctDNA  
101 positivity after surgery is associated with a higher risk of disease recurrence<sup>10,11</sup>. Previous

102 studies have shown that this correlation had already been found as early as four weeks after  
103 primary tumor resection<sup>12</sup>. However, ctDNA analysis alone does not capture the  
104 morphological characteristic of the tumor. For instance, information such as histopathological  
105 subtype, grading, vascular and lymphatic invasion, as well as the abundance of tumor-  
106 infiltrating lymphocytes<sup>13-16</sup>, among many other morphological properties of the tumor  
107 microenvironment (TME), have been shown to be prognostically relevant and are reflected in  
108 current clinical guidelines<sup>17,18</sup>. Deep Learning (DL) is an artificial intelligence technology  
109 which is useful to extract quantitative biomarkers from routinely available clinical data in  
110 oncology<sup>19,20</sup>. DL models, trained on histopathological routine hematoxylin and eosin (H&E)  
111 tumor slides have been shown to act as survival prediction models outperforming current  
112 risk-stratifications systems<sup>21-23</sup>. DL can extract highly relevant information from routine  
113 pathology slides of CRC, including presence of microsatellite instability (MSI)<sup>24,25</sup>, gene  
114 mutations<sup>25,26</sup>, response to neoadjuvant therapy<sup>27</sup>, and overall survival (OS)<sup>22</sup>. Given the  
115 ability of DL to extract meaningful biological information from pathology slides that ctDNA  
116 cannot capture, we hypothesise that the combination of MRD assessment with a  
117 transformer-based DL risk score from morphology could significantly improve prognosis  
118 prediction. In this study, we aim to enhance patient stratification and recurrence prediction in  
119 patients with CRC by integrating MRD status derived from ctDNA with a DL-based risk score  
120 trained on routine histological images.

## 121 **Methods & Materials**

### 122 **Patient Data Acquisition**

123 In this study, we analysed histological whole slide images (WSIs) of hematoxylin & eosin  
124 (H&E) stained tumour tissue of surgically curable CRC from two large cohorts in Germany  
125 and Japan (Figure 1A-B, Supplementary Figure 1). The first cohort was the Darmkrebs:  
126 Chancen der Verhütung durch Screening Study (DACHS), which includes 1774 WSI's  
127 belonging to 1766 patients and was used as a training cohort (Supplementary Figure 1A).  
128 The second cohort was the GALAXY trial from the CIRCULATE-Japan study  
129 (UMIN000039205), which includes 1556 WSIs from 1555 patients and was used as an  
130 independent external validation cohort (Supplementary Figure 1B). The GALAXY trial  
131 comprised ctDNA data measuring the MRD status at the four weeks post-surgery interval:  
132 MRD positivity was defined as at least 2 out of 16 tumour-specific ctDNA variants detected  
133 above a predefined threshold based on Natera's method<sup>12,28</sup>. Out of the 1555 patients  
134 included in the trial, 241 were MRD-positive and 1314 patients were MRD-negative at the  
135 respective 4 weeks interval<sup>12</sup> (Figure 1B). For both cohorts, disease free survival in months

136 (DFS) was available. DFS marked the time from primary surgery to last follow-up date or last  
137 surgery to last follow-up date for patients for which primary surgery date was unavailable.

## 138 **Image Processing and Deep Learning Techniques**

### 139 **Data Preprocessing**

140 All whole-slide images (WSIs) were segmented into image patches with dimensions of  
141  $224 \times 224$  pixels and an edge length of  $256 \mu\text{m}$ , resulting in an effective magnification of  
142  $1.14 \mu\text{m}$  per pixel. During this segmentation process, patches that primarily contained  
143 background or blur (identified by having an average number of Canny edges below a  
144 threshold of 2) were removed from the dataset. The retained image tiles were colour  
145 normalised using the Macenko method in order to avoid stain-associated bias<sup>29</sup>. For WSI  
146 pre-processing, we employed our end-to-end publicly available pipeline, which can be found  
147 here: <https://github.com/KatherLab/end2end-WSI-preprocessing>.

148

### 149 **Model Development**

150 To train and validate our prediction DL-models we used our open-source pipeline, marugoto  
151 (<https://github.com/KatherLab/marugoto>). In the initial step, a self-supervised learning (SSL)  
152 model called UNI, pretrained on over 100 M histology-specific images and 100k WSIs, was  
153 employed to extract a 1024-dimensional feature vector from each image tile (Figure 1A-B)<sup>30</sup>.  
154 The obtained features were then preprocessed using a multi-headed self-attention  
155 mechanism by the transformer network (Figure 1C). Here, the network views patch  
156 embeddings as a sequence, with elements interacting through self-attention. For a WSI with  
157  $n$  patches of dimension  $d$ , self-attention calculates a query-key product. Multi-headed self-  
158 attention repeats this in  $h$  heads, then concatenating and transforming the outputs. The  
159 transformer architecture is designed with two layers, each featuring eight heads (total  $h=8$ ),  
160 a latent dimension of 512, and equal dimensions (each 64) for queries, keys, and values.  
161 Post self-attention, the embeddings of each patch are combined into a sequence of  
162 dimension  $n \times 1024$  processed through a linear projection and ReLU activation to reduce  
163 dimensionality to 512. A learnable class token is added to this sequence, resulting in an  
164 input dimension of  $(n+1) \times 512$  that is fed into the transform layer. Each transformer layer  
165 consists of a layer normalisation block followed by multi-headed self-attention, a block of  
166 layer normalisation and finally a multi-layer perceptron (MLP), with skip connections  
167 integrated across each block to facilitate training<sup>24</sup>. After processing through two transformer  
168 layers, the class token is inputted into an MLP head designed to produce a continuous risk  
169 score for each patient, serving as the output of the model. For model training, we used Cox  
170 partial likelihood, as the loss function<sup>22,31</sup>. We randomly split the DACHS cohort at the patient

171 level into training, validation, and test sets in a 4:4:2 ratio. The model was trained using the  
172 training set, and the best checkpoint, determined by the highest C-index on the validation  
173 set, was saved. This checkpoint was then validated on DACHS test set and CIRCULATE  
174 data cohort

175

## 176 **Visualisation**

177 To interpret our model's output, we generated whole-slide patient heatmaps showing the DL  
178 prediction scores. We used our trained Vision Transformer (ViT) model to process tile-level  
179 features extracted from the WSI. The features are passed through the trained model to  
180 obtain tile-level scores, which are then combined with Grad-CAM (Gradient-weighted Class  
181 Activation Mapping) values to generate weighted scores, which were normalised to a range  
182 of -1 to 1 facilitating the identification of the most significant tiles. Heatmaps were then  
183 created using the weighted scores, with red indicating high-risk, and blue indicating low-risk.  
184 To maintain interpretability, we blended these heatmaps with the original image features,  
185 providing clear insights into the tumor morphology and the model's predictions.

## 186 **Experimental Design**

187 In our study we first trained a transformer-based DL model on the DACHS cohort, utilizing  
188 clinical data on disease-free survival (DFS) events and DFS time in months to generate  
189 patient level DL-based risk scores (Figure 1C). Next, we externally validated the trained DL  
190 model on the GALAXY cohort. The continuous DL-risk score was binarized into DL high-risk  
191 and DL low-risk categories based on a fixed threshold, defined as the median risk score in  
192 the training cohort (0.9357855). Subsequently, we combined the four-week post-surgery  
193 MRD status from the GALAXY trial with the DL-risk scores to analyze survival differences  
194 between these subgroups (Figure 1D). We also looked at the effects of adjuvant  
195 chemotherapy in the various subgroups. Survival Analysis was performed using Kapan-  
196 Meier analysis and log-rank test to compare DFS time between the groups. Additionally,  
197 multivariate analysis was conducted using Cox proportional hazard models, including the  
198 covariates: age, gender, pathological T-Stage (pT) and pathological N-Stage (pN)<sup>22</sup>. Lastly,  
199 we performed a morphological analysis to identify histopathological correlations between the  
200 DL high-risk and low-risk subgroups, using classification heatmaps (Figure 1D).

## 201 **Data and Code availability**

202 Our whole slide image preprocessing pipeline is available here:  
203 <https://github.com/KatherLab/end2end-WSI-preprocessing>. The code for the pretrained  
204 vision encoder UNI can be found under: <https://github.com/mahmoodlab/uni>. Our DL model



205 codes are publicly available at [https://github.com/KatherLab/marugoto/tree/survival-](https://github.com/KatherLab/marugoto/tree/survival-transformer/marugoto/survival)  
206 [transformer/marugoto/survival](https://github.com/KatherLab/marugoto/tree/survival-transformer/marugoto/survival). The respective study Principal Investigators provided the  
207 remaining data. For detailed data sharing policies, please refer to the original publications.

## 208 **Results**

### 209 **DL stratifies patients by recurrence risk**

210 We trained a DL model to generate risk scores based on DFS and validated its performance  
211 on the GALAXY cohort. Based on the DL-risk scores, we divided our cohort into DL high-  
212 and DL low-risk groups, followed by a survival analysis using Kaplan Meier estimator and  
213 Cox proportional hazard analysis (Figure 1D). These results were then compared with the  
214 stratification outcomes of MRD status four weeks post-surgery in the GALAXY cohort.  
215 Among the 1,555 patients 19.8% (n=307) were categorized as DL high-risk and 80.2%  
216 (n=1248) as DL low-risk. Patients classified as DL high-risk exhibited a significantly elevated  
217 risk of disease recurrence compared to DL low-risk patients (HR=2.6, CI 95% 2.11-3.21;  $p <$   
218 0.005), with a 20-month DFS of 59.3% vs. 82.1%, respectively (Figure 1D). The ctDNA  
219 analysis alone stratified 15.5 % (n=241) patients as MRD-positive and 84.5% (n=1,314) as  
220 MRD-negative, with an HR of 11.4 (CI 95% 9.28-14,  $p < 0.001$ , Supplementary Figure 2A). In  
221 the multivariate analysis, including the covariates age, sex, pT, and pN, we found the most  
222 prognostic indicator for recurrence risk to be MRD positivity (HR=10.57, CI 95% 8.26-13.53;  
223  $p < 0.001$ ), followed by pT3-pT4-Stage (HR=2.00, CI 95% 1.20-3.35;  $p < 0.05$ , Figure 1F). The  
224 DL-risk score was significant with an HR of 1.46 (CI 95% 1.11-1.90,  $p < 0.05$ ). When  
225 correlating the DL risk categories with patient characteristics, we found significant  
226 differences in sex, pT-Stage, pN-Stage, pathological Stage, and MRD status (Table 1).  
227 Together, these data demonstrate that the DL model can significantly stratify patients  
228 according to their risk of recurrence.

### 229 **DL stratifies recurrence risk within MRD subgroups**

230 We hypothesised that by integrating the MRD status with our DL risk score we can further  
231 stratify the patients according to risk of recurrence, particularly the MRD-negative patients.  
232 To test this, we combined the binarized DL-derived risk score with the MRD status four-  
233 weeks after curative surgery (Figure 2). In the MRD-positive group, 33.6% (81 out of 241  
234 patients) were categorized as DL high-risk and 66.4% (160 out of 241 patients) as DL low-  
235 risk, with an HR of 1.57 (CI 95% 1.18-2.12;  $p = 0.002$ , Figure 2A). The DFS-time interval was  
236 longer in the DL low-risk group, with a 20-months DFS of 30.9% compared to 9.9% in the DL  
237 high-risk group (Figure 2A).

238 In the MRD-negative group, 17.2% (226 out of 1,314 patients) were classified as high-risk by  
239 the DL model and 82.8% (1,088 out of 1,314 patients) as DL low-risk with an HR of 2.36 (CI  
240 95% 1.73-3.23;  $p < 0.001$ , Figure 2B). Additionally, the 20-month DFS was longer in the DL  
241 low-risk group at 89.7%, compared to 77% in the DL high-risk group (Figure 2B). In a  
242 multivariate Cox analysis with age, sex, pT and pN as covariates, the DL-score was the only  
243 independent prognostic predictor in the MRD-positive group with an HR of 1.51 (CI 95%  
244 1.07-2.14;  $p = 0.018$ , Supplementary Figure 2B). In the MRD-negative group, pT1-T2 was the  
245 strongest prognostic indicator with an HR of 2.50 (CI 95% 1.73-3.64;  $p < 0.001$ ,  
246 Supplementary Figure 2C). The DL risk score, with an HR of 1.28 (CI 95% 0.83-1.99;  
247  $p = 0.27$ ), was not an independent prognostic predictor (Supplementary Figure 2C). In  
248 summary, these data show that the combination of MRD status with the DL risk score  
249 enables a better stratification of patients with CRC.

## 250 **DL-based recurrence risk predicts benefit from adjuvant chemotherapy** 251 **in MRD-negative patients**

252 We hypothesised that our DL-risk score could identify patients with stage II-IV CRC who  
253 might benefit from ACT, despite being MRD-negative. To test this hypothesis, we explored  
254 the association of ACT with DFS by performing Kaplan-Meier analysis within the DL high-risk  
255 and low-risk subgroups among both MRD-positive and MRD-negative patients (Figure 2 C-  
256 F). For the MRD-positive group, patients receiving ACT had significantly longer DFS in  
257 both the DL low-risk group (HR=0.20, CI 95% 0.14-0.30;  $p < 0.001$ , Figure 2C) and in the DL  
258 high-risk group (HR=0.25, CI 95% 0.16-0.43;  $p < 0.001$ , Figure 2E). Without receiving ACT, all  
259 MRD-positive and DL high-risk patients experienced recurrence within 20-months, whereas  
260 18.6% of the MRD-positive and DL high-risk patients who received ACT remained disease-  
261 free after 20 months (Figure 2E). In the MRD-negative group, patients in the low-risk DL  
262 group did not have longer DFS when treated with ACT (HR=1.14, CI 95% 0.8-1.63;  $p = 0.48$ ).  
263 The 20-month DFS was 89.4% for patients treated with ACT vs 89.9% for patients not  
264 receiving ACT (Figure 2D). Interestingly, patients in the MRD-negative and DL high-risk  
265 group showed significantly longer DFS when treated with ACT (HR 0.48, CI 95% 0.27-0.86;  
266  $p = 0.01$ , Figure 2D). The 20-month DFS rate was 86.2% in patients who received ACT and  
267 thus significantly higher than in patients who did not receive ACT (70.5%). This disease-free  
268 survival advantage continued to be seen in the 40-month DFS rate at 83% (with ACT) vs  
269 68.9% (without receiving ACT, Figure 2F).

270 Together, these data show that the DL prognostication model can successfully further stratify  
271 MRD-negative patients. This indicated that even within the low-risk subgroup (according to



272 MRD), there are high-risk individuals for whom the omission of ACT may carry a higher risk  
273 of recurrence.

## 274 **DL can identify histopathological features linked to prognosis**

275 Measurements of ctDNA provide information about viable and disseminated tumor cells,  
276 serving as surrogate markers for their presence in the body and enabling a non-invasive  
277 assessment of MRD after surgery. However, they do not provide any information regarding  
278 tumor morphology as well as the TME, which is reflected in histopathology slides and is  
279 known to be related to clinical outcomes. We investigated whether our model trained on  
280 histopathology images without any manual annotation, learned to consider morphological  
281 features of the tumor and the TME, which would be synergistic to MRD status. We used a  
282 model trained on DACHS and deployed on GALAXY, visualising highly predictive regions at  
283 both high and low magnification, as shown in Figure 3.

284 In the DL low-risk classified patients, the morphological analysis revealed a variety of benign  
285 histopathological tissue features (Supplementary Figure 3A). As the DL score increased, the  
286 histological image tiles still below the risk threshold displayed moderately differentiated  
287 tumor components. These samples still displayed a balanced tumor-stroma ratio and tumor  
288 glands with tubular to cribriform architecture, indicating an intermediate phenotype between  
289 DL low and DL high-risk morphological characteristics (Figure 3A-B). The images, above the  
290 risk threshold, displayed high-grade tumor cells with a significant desmoplastic stroma  
291 reaction. There was a high intratumoral stroma fraction, and the presence of tumor  
292 buds/poorly differentiated clusters, which are known to be associated with a higher  
293 recurrence risk (Figure 3A-B).<sup>32-36</sup> Taken together, we observed a clear morphological  
294 continuum mirroring the progression from DL low to DL high-risk tumors. Moreover, we  
295 analysed the distribution of the DL risk score with clinically relevant molecular information  
296 namely MSI status, *BRAF* and *RAS* mutational status (Figure 3 C-F). We found that the  
297 distribution was very similar for all these factors, suggesting that our DL model  
298 independently detects and accounts for additional prognostically relevant morphological  
299 features.

300 In summary, although our histopathology DL model was trained without human annotations,  
301 and solely on non-processed WSIs, we found that the model learned to pay attention to  
302 regions linked to tumor biological features plausibly associated with prognosis, thereby  
303 synergizing with ctDNA. Moreover, our findings are consistent with previous DL-based end-  
304 to-end prognostication approaches in CRC based on H&E histopathology alone<sup>22,37</sup>.

## 305 **Discussion**

306 CRC can often be cured through surgery, but a subset of patients experience relapse, which  
307 is associated with high mortality. To mitigate this risk, ACT is administered to locally  
308 advanced CRC patients post-surgery. However, the majority of these patients do not benefit  
309 from such treatment, which is associated with substantial side effects<sup>38</sup>. Decades of research  
310 have focused on identifying potential biomarkers to administer ACT selectively to high-risk  
311 individuals who would benefit the most, while withholding it from low-risk individuals. To  
312 date, one of the most promising biomarkers for this purpose is ctDNA. Measurement of MRD  
313 through ctDNA is non-invasive, robust, and highly prognostic. However, ctDNA does not  
314 capture the tumor's interaction with its microenvironment—the complex spatial ecology of  
315 tumors<sup>39</sup>-nor the tumor morphology itself. This is a limitation of ctDNA as a biomarker given  
316 that, in addition to conventional histopathology tumor features, the interplay between tumors  
317 and their microenvironment has been demonstrated to be highly prognostic and predictive  
318 over the years. In our study, we demonstrate that combining DL-based risk assessment with  
319 MRD measurement further enhances prognostic capabilities: MRD-negative patients who  
320 were predicted to be at high-risk for relapse by our DL model had a significantly longer DFS  
321 if treated with ACT, whereas in MRD-negative patients with a DL-based low-risk status no  
322 DFS benefit was seen for those receiving ACT (Figure 2F). These observations suggest that  
323 healthcare providers may identify a subset of patients who are at risk for relapse but are not  
324 detected through current diagnostic tools, including a diagnostic as innovative as ctDNA.  
325 Previous studies developing DL-based prognostication systems failed to provide evidence  
326 for potentially different chemotherapy efficacy across DL categories, by which all potential  
327 therapeutic implications of these models remain speculative<sup>23,40</sup>

328 To our knowledge, our study provides the first evidence suggesting that a DL risk  
329 assessment algorithm may indicate therapy efficacy in a real world setting in CRC. This  
330 combined approach may improve patient selection, suggesting a way how ACT could be  
331 restricted to those patients who are most likely to benefit from it. Furthermore, our DL  
332 method is using the latest state-of-the-art models, is fully open source and can be reused  
333 and adapted by anyone.

## 334 **Limitations**

335 A limitation of our study is that integrating our insights into clinical routine requires further  
336 evaluation in additional cohorts, ideally in a prospective manner. Despite this, our study,  
337 encompassing thousands of patients across different ethnicities, represents one of the  
338 largest studies in this field. Moreover, we utilized a state-of-the-art foundation model for

339 digital pathology analysis, UNI<sup>30</sup>. This is particularly relevant for clinical translatability, as the  
340 capabilities of foundation models are rapidly advancing, suggesting that further performance  
341 gains are conceivable with improved DL models. Nevertheless, medical device approval in  
342 Japan, the US, and the European Union requires a static piece of software that cannot be  
343 easily updated. Therefore, like any other DL-based biomarker, our method may be outdated  
344 by the time of clinical approval. We urge regulators and policymakers to work towards  
345 enabling the update of DL-based biomarkers with the latest technologies.

## 346 **Conclusion**

347 Despite these limitations, our data show that the excellent prognostic performance of ctDNA  
348 in CRC can be further improved by DL-based end-to-end assessment of routine pathology  
349 slides. After prospective validation, this approach provides a plausible and comprehensive  
350 strategy for relapse risk assessment with potential therapeutic implications.

## 351 **Funding**

352 JNK is supported by the German Cancer Aid (DECADE, 70115166), the German Federal  
353 Ministry of Education and Research (PEARL, 01KD2104C; CAMINO, 01EO2101; SWAG,  
354 01KD2215A; TRANSFORM LIVER, 031L0312A; TANGERINE, 01KT2302 through ERA-NET  
355 Transcan), the German Academic Exchange Service (SECAI, 57616814), the German  
356 Federal Joint Committee (TransplantKI, 01VSF21048) the European Union's Horizon Europe  
357 and innovation programme (ODELIA, 101057091; GENIAL, 101096312), the European  
358 Research Council (ERC; NADIR, 101114631) and the National Institute for Health and Care  
359 Research (NIHR, NIHR203331) Leeds Biomedical Research Centre. The views expressed  
360 are those of the author(s) and not necessarily those of the NHS, the NIHR or the Department  
361 of Health and Social Care. This work was funded by the European Union. Views and  
362 opinions expressed are however those of the author(s) only and do not necessarily reflect  
363 those of the European Union. Neither the European Union nor the granting authority can be  
364 held responsible for them. CIRCULATE-Japan receives financial support from the Japan  
365 Agency for Medical Research and Development (grant 19ck0106447h0002-TY). SF is  
366 supported by the German Federal Ministry of Education and Research (SWAG,  
367 01KD2215A), the German Cancer Aid (DECADE, 70115166 and TargHet, 70115995) and  
368 the German Research Foundation (504101714). The DACHS study (HB, TY, DW and MH)  
369 was supported by the German Research Council (BR 1704/6-1, BR 1704/6-3, BR 1704/6-4,  
370 CH 117/1-1, HO 5117/2-1, HO 5117/2-2, HE 5998/2-1, HE 5998/2-2, KL 2354/3-1, KL  
371 2354/3-2, RO 2270/8-1, RO 2270/8-2, BR 1704/17-1 and BR 1704/17-2), the  
372 Interdisciplinary Research Program of the National Center for Tumor Diseases (NCT;

373 Germany) and the German Federal Ministry of Education and Research (01KH0404,  
374 01ER0814, 01ER0815, 01ER1505A and 01ER1505B).

375

## 376 **Disclosures**

377 **CMLL** reports honoraria from AstraZeneca. **HB** reports research funding from Ono  
378 Pharmaceutical and honoraria from Ono Pharmaceutical, Eli Lilly Japan, and Taiho  
379 Pharmaceutical. **TM** reports honoraria from Chugai, AstraZeneca, and Miyarisan. **SM** reports  
380 honoraria from Taiho Pharmaceutical Co., Ltd., Chugai Pharmaceutical Co., Ltd., and Eli  
381 Lilly CO, Ltd. **DK** reports honoraria from Takeda, Chugai, Lilly, MSD, Ono, Seagen,  
382 Guardant Health, Eisai, Taiho, Bristol Myers Squibb, Daiichi-Sankyo, Pfizer,  
383 Merckbiopharma, and Sysmex: research funding from Ono, MSD, Novartis, Servier,  
384 Janssen, IQVIA, Syneoshealth, CIMIC, and Cimicshiftzero. **HT** reports speakers' bureau  
385 from MSD K.K, Merck Biopharma, Takeda, Taiho, Lilly Japan, Bristol-Myers Squibb Japan,  
386 Chugai Pharmaceutical, Ono Yakuhin, Amgen; research funding from Takeda, Daiichi  
387 Sankyo. **IT** reports speakers' bureau from Medtronic, Johnson & Johnson, Intuitive,  
388 Medcaroid, Eli Lilly and research funding from Medtronic, sysmex. **SF** has received  
389 honoraria from MSD and BMS. **TK** reports nothing to declare. **EO** reports speakers' bureau  
390 from Chugai Pharmaceutical Co., Ltd., Bristol Meyers, Ono Pharmaceutical Co., Ltd., Eli  
391 Lilly, Takeda Pharmaceutical Co., Ltd.; research funding from Guardant Health, Inc.;  
392 advisory role from Glaxosmithkline plc. **YN** reports advisory role from Guardant Health Pte  
393 Ltd., Natera, Inc., Roche Ltd., Seagen, Inc., Premo Partners, Inc., Daiichi Sankyo Co., Ltd.,  
394 Takeda Pharmaceutical Co., Ltd., Exact Sciences Corporation, and Gilead Sciences, Inc.;  
395 speakers' bureau from Guardant Health Pte Ltd., MSD K.K., Eisai Co., Ltd., Zeria  
396 Pharmaceutical Co., Ltd., Miyarisan Pharmaceutical Co., Ltd., Merck Biopharma Co., Ltd.,  
397 CareNet, Inc., Hisamitsu Pharmaceutical Co., Inc., Taiho Pharmaceutical Co., Ltd., Daiichi  
398 Sankyo Co., Ltd., Chugai Pharmaceutical Co., Ltd., and Becton, Dickinson and Company,  
399 Guardant Health Japan Corp; research funding from Seagen ,Inc., Genomedica Inc.,  
400 Guardant Health AMEA, Inc., Guardant Health, Inc., Tempus Labs, Inc., Roche Diagnostics  
401 K.K., Daiichi Sankyo Co., Ltd., and Chugai Pharmaceutical Co., Ltd.. **TY** reports honoraria  
402 from Taiho, Chugai, Eli Lilly, Merck, Bayer Yakuhin, Ono and MSD, and research funding  
403 from Ono, Sanofi, Daiichi Sankyo, Parexel, Pfizer, Taiho, MSD, Amgen, Genomedica,  
404 Sysmex, Chugai and Nippon Boehringer Ingelheim. S.S. The remaining authors declare no  
405 competing interests. **JNK** declares consulting services for Owkin, France; DoMore  
406 Diagnostics, Norway; Panakeia, UK; Scailyte, Switzerland; Mindpeak, Germany; and  
407 MultiplexDx, Slovakia. Furthermore he holds shares in StratifAI GmbH, Germany, has

408 received a research grant by GSK, and has received honoraria by AstraZeneca, Bayer,  
409 Eisai, Janssen, MSD, BMS, Roche, Pfizer and Fresenius. All the other authors report  
410 nothing to declare.

#### 411 **Ethics statement**

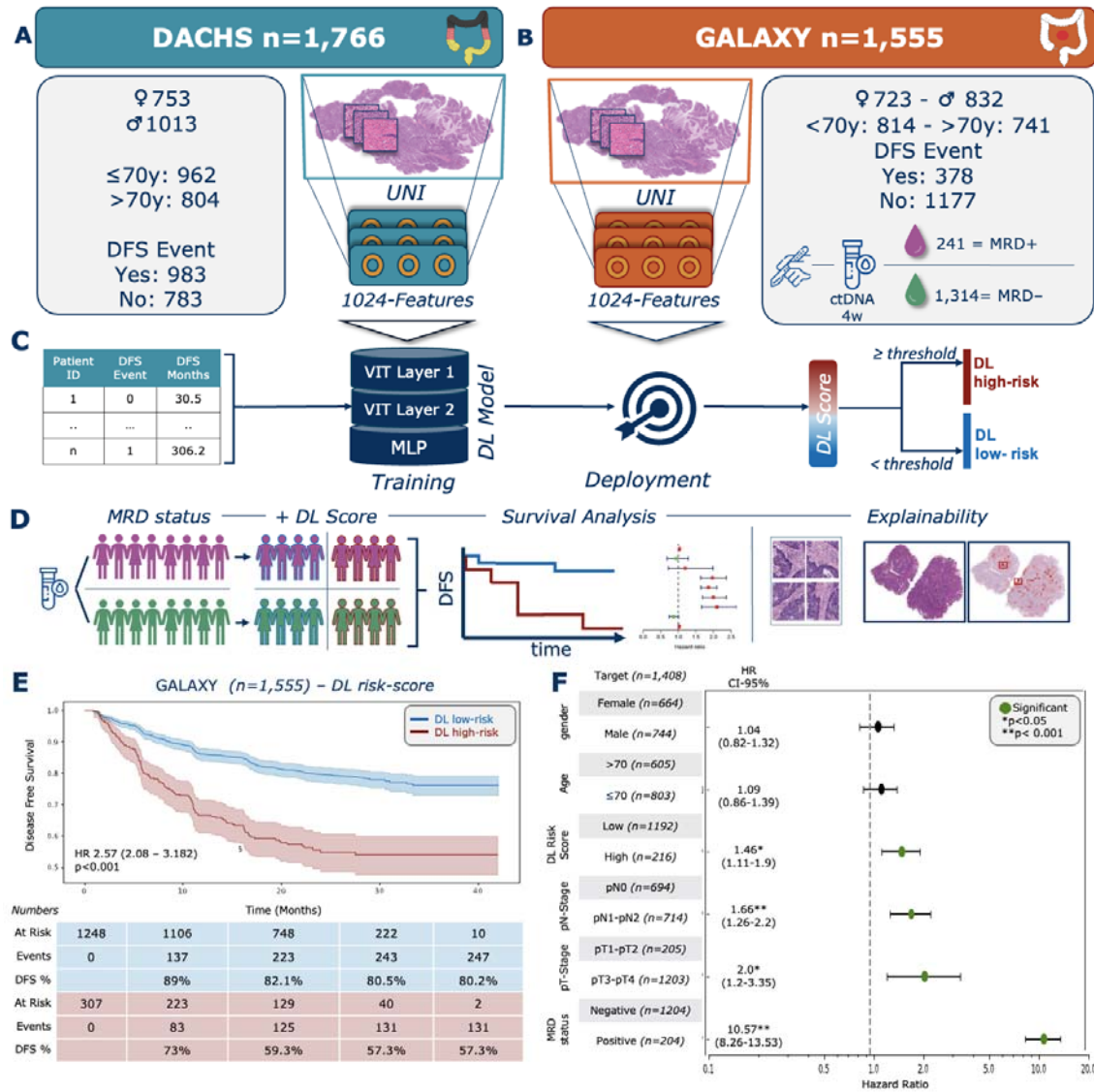
412 The experiments in this study were carried out according to the Declaration of Helsinki and  
413 the International Ethical Guidelines for Biomedical Research Involving Human Subjects by  
414 the Council for International Organizations of Medical Sciences (CIOMS). The present study  
415 also adheres to the “Transparent reporting of a multivariable prediction model for individual  
416 prognosis or diagnosis” (TRIPOD) statement.<sup>20</sup> The Ethics Board at the Medical Faculty of  
417 Technical University Dresden (BO-EK-444102022) and Institutional Review Board of the  
418 National Cancer Center Japan (2023-207) approved of the overall analysis in this study. The  
419 patient sample collection in each cohort was separately approved by the respective  
420 institutional ethics board.

#### 421 **Author contributions**

422 CMLL, HB, JNK and TY conceptualised the study. HD, TN, TM, SM, DK, HT, IT, TK, EO  
423 provided clinical and scanned whole slide image data for the GALAXY cohort. TY, DW, MH,  
424 HB provided clinical and scanned whole slide image data for the DACHS cohort. CMLL  
425 curated the source data. SS, XJ, MvT implemented the deep learning algorithm. SS  
426 developed the code for data analysis and visualisation. CMLL and SS planned and  
427 conducted the experiments. CMLL interpreted the data. HSM, ZIC, JNK assisted with the  
428 interpretation of results. NR and SF did the pathological interpretation of the results. CMLL  
429 wrote the first draft of the manuscript. All authors revised the manuscript draft, contributed to  
430 the interpretation of the data and agreed to the submission of this paper.

431

432 **Figures & Tables**



433

434 **Figure 1: Study Design and DL risk stratification overall**

435 (A) DACHS cohort overview including patient characteristics and WSI preprocessing pipeline  
 436 using UNI a pretrained vision encoder for feature extraction. (B) GALAXY cohort overview  
 437 including patient characteristics and WSI preprocessing pipeline. (C) Flowchart of the study  
 438 design: DFS data was analysed using a Cox-Regression model and fed into the DL-Model  
 439 combined with the image features from the DACHS cohort for training. The DL-Model was  
 440 then deployed onto the GALAXY features and a DL-Score was obtained. (D) Overview  
 441 Experimental Setup: Patients were first categorised based on MRD status and then sub-  
 442 categorized according to the DL score. Survival analysis with Kaplan-Meier estimator and  
 443 Cox proportional hazard models were performed. Lastly, highly predictive Tiles and patient



444 whole slide heatmaps were generated. (E) Kaplan-Meier curves for DFS stratified by DL  
 445 high-risk and DL low-risk patients. (F) Forest plot showing multivariate cox regression  
 446 analysis including the covariates gender, age, DL risk score, pathological Nodal Stage (pN-  
 447 Stage), pathological Tumor Stage (pT-Stage) and MRD-status and their association with  
 448 DFS. HR and 95% CI were calculated by the Cox proportional hazard model. *P*-value was  
 449 calculated using the two-sided log-rank test (\**p*<0.05, \*\* *p*<0.001). Plot were generated  
 450 using lifelines package in Python 3.11.5  
 451 DACHS=Darmkrebs: Chancen der Verhütung durch Screening Study, WSI=whole-slide  
 452 image, DFS=disease-free survival, DL=Deep Learning, MRD=molecular residual disease,  
 453 HR=Hazard ratio, CI=Confidence interval

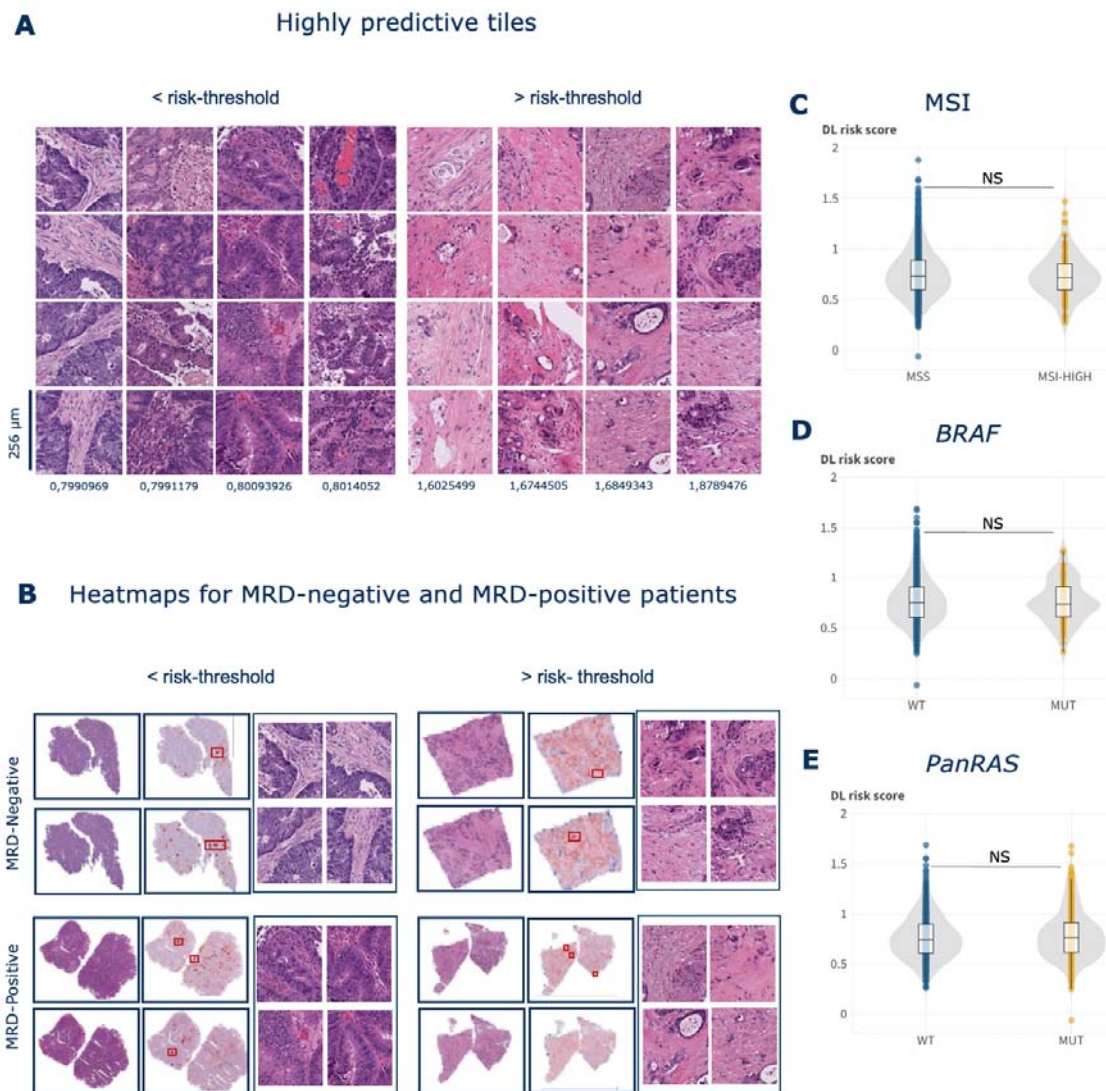


454

455

456 **Figure 2: DL stratifies recurrence risk within MRD subgroups**

457 Kaplan-Meier curves showing DFS stratification by DL high-risk and DL low-risk groups for  
458 (A) MRD-positive and (B) MRD-negative groups, followed by Kaplan-Meier curves showing  
459 DFS stratified by with or without ACT treatment in (C) MRD-positive and DL low-risk, (D)  
460 MRD-negative and DL low-risk, (E) MRD-positive and DL high-risk and (F) MRD-negative  
461 and DL low-risk subgroups. HR and 95% CI were calculated by the Cox proportional hazard  
462 model. *P*-value was calculated using the two-sided log-rank test. Plots were generated using  
463 the lifelines package in Python 3.11.5 DFS=disease-free survival, DL=Deep Learning,  
464 ACT=adjuvant chemotherapy, MRD=molecular residual disease, HR=Hazard ratio,  
465 CI=Confidence interval.  
466



467

468 **Figure 3: Morphological and molecular features of the DL risk score**

469 (A) Highly predictive tiles for patients below the DL risk-threshold and above the DL risk-  
 470 threshold exemplarily with DL score reported. (B) Whole slide patient heatmaps showing the  
 471 DL prediction score, red indicating high-risk, and blue indicating low-risk. Box plot showing  
 472 distribution of DL risk score among (C) MSI status (D) *BRAF-V600E* mutational status and  
 473 (E) *PanRAS* mutational status. *P*-Value calculated using Kruskal-Wallis test. Figure was  
 474 created using Flourish (<https://flourish.studio/>).

475 DL= Deep Learning, MRD= molecular residual disease, WT= wildtype, MUT=mutation,  
 476 MSS=microsatellite stable, MSI= microsatellite instability, NS=not significant

477

478

Patient characteristics	Category	DL high-risk (n=307□), n (%)	DL low-risk (n=1248), n (%)	Chi squared and p values
Age	<=70	167 (54.4)	647 (51.8)	X <sup>2</sup> = 0.54618 P-value = 0.4599
	>70	140 (45.6)	601 (48.2)	
Sex	Female	120 (39.1)	603 (48.3)	X <sup>2</sup> = 8.0696 P-value = 0.004501
	Male	187 (60.9)	645 (51.7)	
ECOG performance Status	0	280 (91.2)	1124 (90)	X <sup>2</sup> = 0.24735 P-value = 0.6189
	1	27 (8.8)	124 (10)	
pT-Stage	T1-T2	10 (3.3)	195 (15.6)	X <sup>2</sup> = 19.26 P-value<0.001
	T3-T4	206 (67.1)	998 (80)	
	NA	91 (29.6)	55 (4.4)	
pN-Stage	N0	76 (35.2)	618 (51.8)	X <sup>2</sup> = 19.646 P-value<0.001
	N1-2	140 (64.8)	574 (48.2)	
	NA	91 (29.6)	56 (4.5)	
pathological Stage	I	3 (1)	148 (11.9)	X <sup>2</sup> = 201.46 P-value<0.001
	II	65 (21.1)	452 (36.2)	
	III	116 (37.8)	533 (42.7)	
	IV	123 (40.1)	115 (9.2)	
RAS status	RAS wild-type	102 (54.8)	394 ( )	X <sup>2</sup> = 0.32606 P-value=0.568
	RAS mutant	84 (45.2)	291 ( )	

	NA	121 (39.4)	563 (45.1)	
<b>BRAF status</b>	<i>BRAF</i> wild-type	171 (55.7)	623 (49.9)	$X^2 = 1.2724e-28$ <i>P</i> -value=1
	<i>BRAF</i> mutant	13 (4.2)	48 (3.8)	
	NA	123 (40.1)	577 (46.2)	
<b>MSI status</b>	MSI	20 (6.5)	102 (8.2)	$X^2 = 0.46606$ <i>P</i> -value=0.4948
	MSS	262 (85.3)	1090 (87.3)	
	NA	25 (8.1)	56 (4.5)	
<b>MRD Status</b>	MRD-positive	81 (26.4)	160 (12.8)	$X^2 = 33.585$ <i>P</i> -value <0.001
	MRD-negative	226 (73.6)	1088 (87.2)	

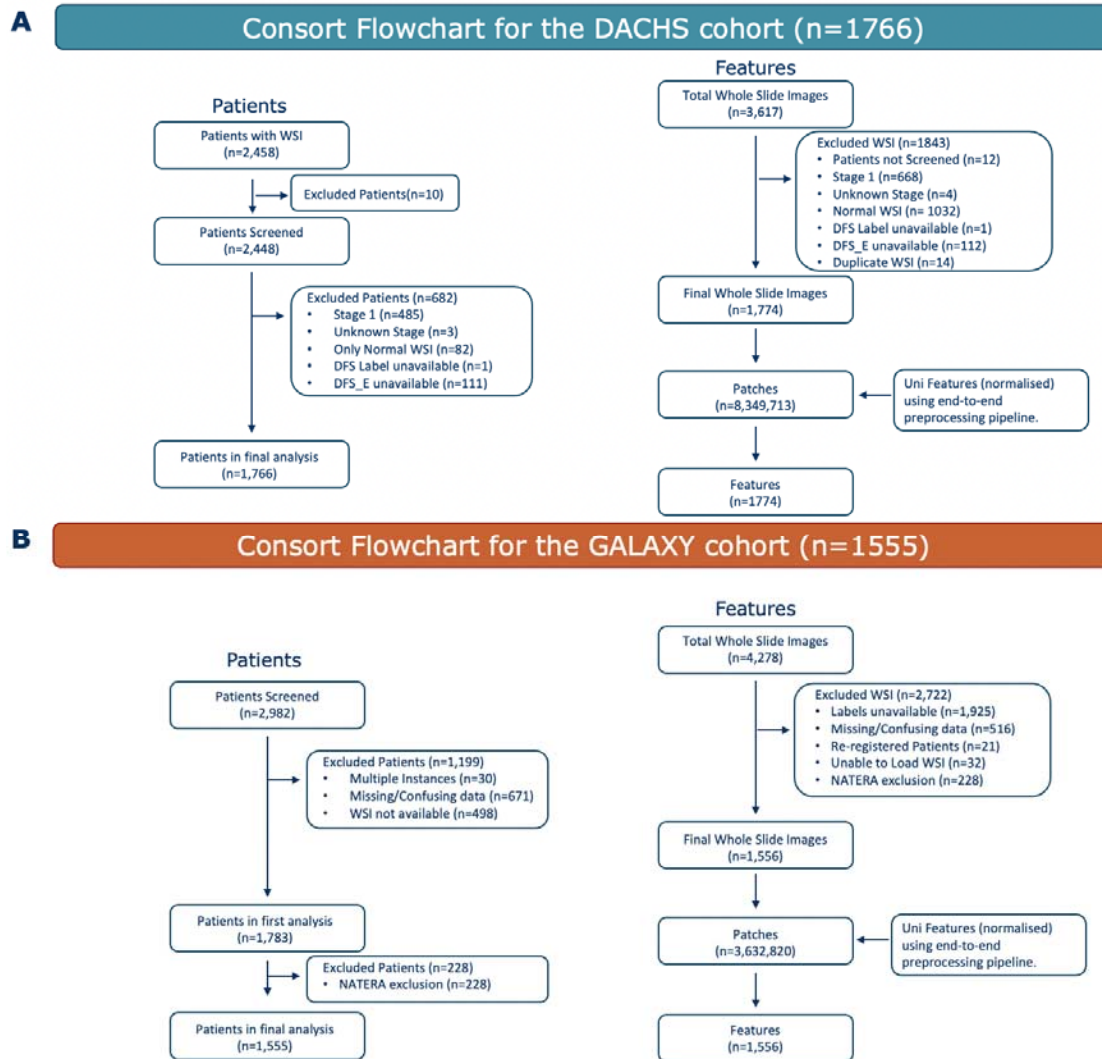
479

480 **Table 1 Patients characteristic for DL high-risk and low-risk patients**

481 P values were obtained by a pearsons chi-squared test with Yates' continuity correction  
 482 comparing the distribution of the factors between the two columns (DL high-risk vs DL low-  
 483 risk). Statistical analysis was performed on R 4.4.4. ECOG=Eastern Cooperativ Oncology  
 484 Group, MSS=microsatellite stable, MSI=microsatellite instable, NA=Not available

485

486 **Supplementary Figures and Tables**



487

488

489 **Supplementary Figure 1: Consort diagram for both cohorts**

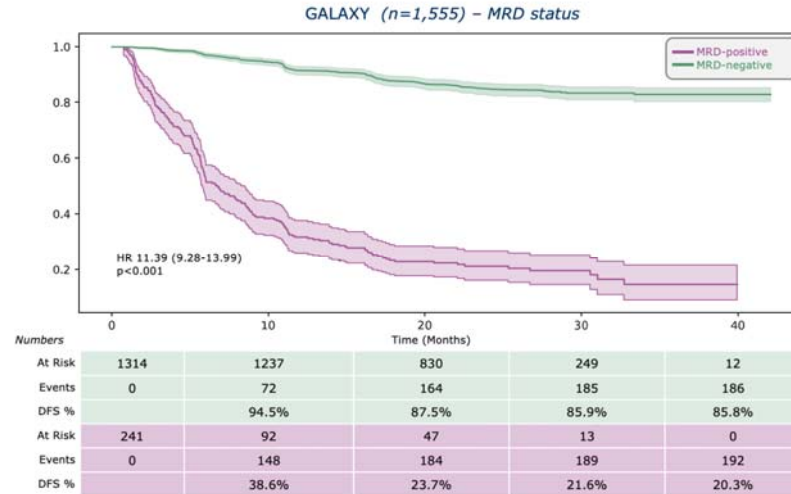
490 Flowchart showing initial screened patients and WSIs and exclusion criterias for (A) the  
 491 DACHS cohort and (B) the GALAXY cohort.

492 WSIs= whole slide images, DACHS=Darmkrebs: Chancen der Verhütung durch Screening

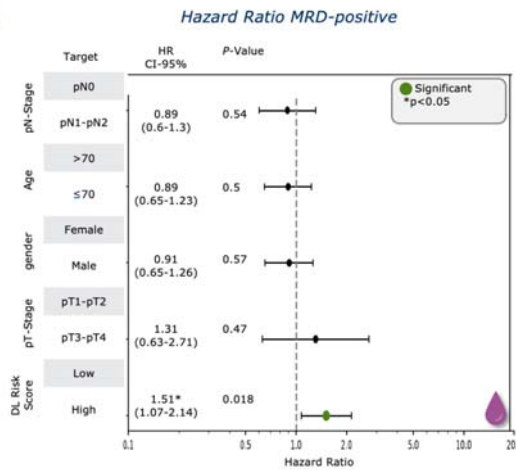
493 Study



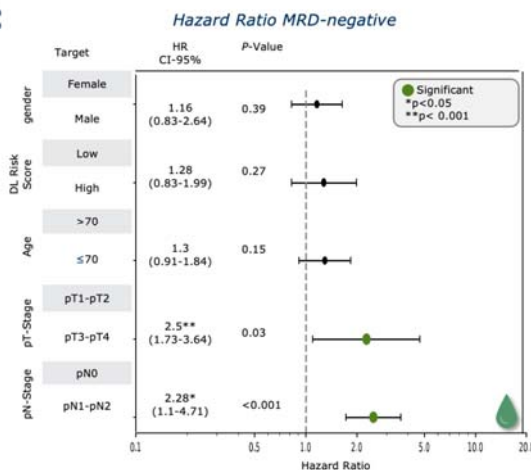
**A**



**B**



**C**



494

495 **Supplementary Figure 2: MRD status is predictive of survival outcomes and**  
 496 **Multivariate analysis for MRD-subgroups**

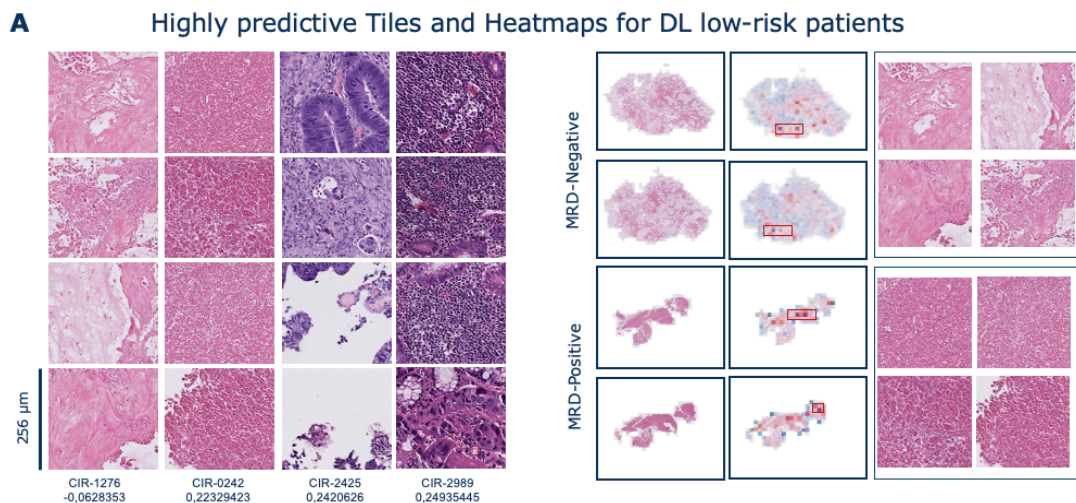
497 (A) Kaplan-Meier curves for DFS stratified by MRD-positive and MRD-negative patients.  
 498 Forest plot showing multivariate cox regression analysis for (B) MRD-positive and (C) MRD-  
 499 negative subgroup including the covariates gender, age, DL risk score, pathological Nodal  
 500 Stage (pN-Stage), pathological Tumor Stage (pT-Stage) and their association with DFS. HR  
 501 and 95% CI were calculated by the Cox proportional hazard model. P-value was calculated  
 502 using the two-sided log-rank test (\*p<0.05, \*\* p<0.001). Plot were generated using lifelines  
 503 package in Python 3.11.5

504 DFS=disease-free survival, DL=Deep Learning, MRD=molecular residual disease,  
 505 HR=Hazard ratio, CI=Confidence interval.

506

507





508

509

### Supplementary Figure 3: Morphological and molecular features for DL low-risk score

510

(A) Highly predictive tiles and Whole slide heatmaps for patients with lowest DL risk score.

511

Red indicating high-risk, and blue indicating low-risk. DL= Deep Learning, MRD= molecular

512

residual disease.

513

514

### Declaration of generative AI and AI-assisted technologies in the writing

515

### process

516

During the preparation of this study the author(s) used GPT-4 for grammar and spelling

517

checking. After using this tool/service, the author(s) reviewed and edited the content as

518

needed and take(s) full responsibility for the content of the publication.

## 519 References

- 520 1. Siegel RL, Giaquinto AN, Jemal A. Cancer statistics, 2024. *CA Cancer J Clin*. January 17,  
521 2024;74(1):12–49.
- 522 2. Boute TC, Swartjes H, Greuter MJE, Elferink MAG, van Eekelen R, Vink GR, et al. Cumulative  
523 Incidence, Risk Factors, and Overall Survival of Disease Recurrence after Curative Resection of  
524 Stage II-III Colorectal Cancer: A Population-based Study. *Cancer Res Commun*. February 29,  
525 2024;4(2):607–616.
- 526 3. Nors J, Iversen LH, Erichsen R, Gotschalck KA, Andersen CL. Incidence of Recurrence and Time  
527 to Recurrence in Stage I to III Colorectal Cancer: A Nationwide Danish Cohort Study. *JAMA*  
528 *Oncol*. January 1, 2024;10(1):54–62.
- 529 4. Liemburg GB, Brandenburg D, Berger MY, Duijts SFA, Holtman GA, de Bock GH, et al.  
530 Diagnostic accuracy of follow-up tests for detecting colorectal cancer recurrences in primary care:  
531 A systematic review and meta-analysis. *Eur J Cancer Care*. September 2021;30(5):e13432.
- 532 5. Nicholson BD, Shinkins B, Pathiraja I, Roberts NW, James TJ, Mallett S, et al. Blood CEA levels  
533 for detecting recurrent colorectal cancer. *Cochrane Database Syst Rev*. December 10,  
534 2015;2015(12):CD011134.
- 535 6. Shinkins B, Nicholson BD, James T, Pathiraja I, Pugh S, Perera R, et al. What carcinoembryonic  
536 antigen level should trigger further investigation during colorectal cancer follow-up? A systematic  
537 review and secondary analysis of a randomised controlled trial. *Health Technol Assess*. April  
538 2017;21(22):1–60.
- 539 7. O'Connor ES, Greenblatt DY, LoConte NK, Gangnon RE, Liou J-I, Heise CP, et al. Adjuvant  
540 chemotherapy for stage II colon cancer with poor prognostic features. *J Clin Oncol*. September 1,  
541 2011;29(25):3381–3388.
- 542 8. Baxter NN, Kennedy EB, Bergsland E, Berlin J, George TJ, Gill S, et al. Adjuvant Therapy for  
543 Stage II Colon Cancer: ASCO Guideline Update. *J Clin Oncol*. March 10, 2022;40(8):892–910.
- 544 9. Moding EJ, Nabet BY, Alizadeh AA, Diehn M. Detecting Liquid Remnants of Solid Tumors:  
545 Circulating Tumor DNA Minimal Residual Disease. *Cancer Discov*. December 1,  
546 2021;11(12):2968–2986.
- 547 10. Kasi PM, Fehringer G, Taniguchi H, Starling N, Nakamura Y, Kotani D, et al. Impact of Circulating  
548 Tumor DNA-Based Detection of Molecular Residual Disease on the Conduct and Design of  
549 Clinical Trials for Solid Tumors. *JCO Precis Oncol*. March 2022;6:e2100181.
- 550 11. Tie J, Cohen JD, Wang Y, Li L, Christie M, Simons K, et al. Serial circulating tumour DNA  
551 analysis during multimodality treatment of locally advanced rectal cancer: a prospective  
552 biomarker study. *Gut*. April 2019;68(4):663–671.
- 553 12. Kotani D, Oki E, Nakamura Y, Yukami H, Mishima S, Bando H, et al. Molecular residual disease  
554 and efficacy of adjuvant chemotherapy in patients with colorectal cancer. *Nat Med*. January  
555 2023;29(1):127–134.
- 556 13. Galon J, Costes A, Sanchez-Cabo F, Kirilovsky A, Mlecnik B, Lagorce-Pagès C, et al. Type,  
557 density, and location of immune cells within human colorectal tumors predict clinical outcome.  
558 *Science*. September 29, 2006;313(5795):1960–1964.
- 559 14. Pagès F, Mlecnik B, Marliot F, Bindea G, Ou F-S, Bifulco C, et al. International validation of the  
560 consensus Immunoscore for the classification of colon cancer: a prognostic and accuracy study.  
561 *Lancet*. May 26, 2018;391(10135):2128–2139.
- 562 15. Jesinghaus M, Schmitt M, Lang C, Reiser M, Scheiter A, Konukiewitz B, et al. Morphology  
563 Matters: A Critical Reappraisal of the Clinical Relevance of Morphologic Criteria From the 2019  
564 WHO Classification in a Large Colorectal Cancer Cohort Comprising 1004 Cases. *Am J Surg*

- 565 *Pathol.* July 1, 2021;45(7):969–978.
- 566 16. Wankhede D, Yuan T, Kloor M, Halama N, Brenner H, Hoffmeister M. Clinical significance of  
567 combined tumour-infiltrating lymphocytes and microsatellite instability status in colorectal cancer:  
568 a systematic review and network meta-analysis. *Lancet Gastroenterol Hepatol.* July  
569 2024;9(7):609–619.
- 570 17. Argilés G, Tabernero J, Labianca R, Hochhauser D, Salazar R, Iveson T, et al. Localised colon  
571 cancer: ESMO Clinical Practice Guidelines for diagnosis, treatment and follow-up†. *Ann Oncol.*  
572 October 1, 2020;31(10):1291–1305.
- 573 18. Roth AD, Delorenzi M, Tejpar S, Yan P, Klingbiel D, Fiocca R, et al. Integrated analysis of  
574 molecular and clinical prognostic factors in stage II/III colon cancer. *J Natl Cancer Inst.* November  
575 7, 2012;104(21):1635–1646.
- 576 19. Shmatko A, Ghaffari Laleh N, Gerstung M, Kather JN. Artificial intelligence in histopathology:  
577 enhancing cancer research and clinical oncology. *Nat Cancer.* September 2022;3(9):1026–1038.
- 578 20. Perez-Lopez R, Ghaffari Laleh N, Mahmood F, Kather JN. A guide to artificial intelligence for  
579 cancer researchers. *Nat Rev Cancer.* May 16, 2024; Available at:  
580 <http://dx.doi.org/10.1038/s41568-024-00694-7>
- 581 21. Muti HS, Röcken C, Behrens H-M, Löffler CML, Reitsam NG, Grosser B, et al. Deep learning  
582 trained on lymph node status predicts outcome from gastric cancer histopathology: a  
583 retrospective multicentric study. *Eur J Cancer.* November 2023;194:113335.
- 584 22. Jiang X, Hoffmeister M, Brenner H, Muti HS, Yuan T, Foersch S, et al. End-to-end  
585 prognostication in colorectal cancer by deep learning: a retrospective, multicentre study. *Lancet*  
586 *Digit Health.* January 2024;6(1):e33–e43.
- 587 23. Kleppe A, Skrede O-J, De Raedt S, Hveem TS, Askautrud HA, Jacobsen JE, et al. A clinical  
588 decision support system optimising adjuvant chemotherapy for colorectal cancers by integrating  
589 deep learning and pathological staging markers: a development and validation study. *Lancet*  
590 *Oncol.* September 2022;23(9):1221–1232.
- 591 24. Wagner SJ, Reisenbüchler D, West NP, Niehues JM, Zhu J, Foersch S, et al. Transformer-based  
592 biomarker prediction from colorectal cancer histology: A large-scale multicentric study. *Cancer*  
593 *Cell.* September 11, 2023;41(9):1650–1661.e4.
- 594 25. Kather JN, Pearson AT, Halama N, Jäger D, Krause J, Loosen SH, et al. Deep learning can  
595 predict microsatellite instability directly from histology in gastrointestinal cancer. *Nat Med.* July  
596 2019;25(7):1054–1056.
- 597 26. Gustav M, Reitsam NG, Carrero ZI, Loeffler CML, van Treeck M, Yuan T, et al. Deep learning for  
598 dual detection of microsatellite instability and POLE mutations in colorectal cancer  
599 histopathology. *NPJ Precis Oncol.* May 23, 2024;8(1):115.
- 600 27. Foersch S, Glasner C, Woerl A-C, Eckstein M, Wagner D-C, Schulz S, et al. Multistain deep  
601 learning for prediction of prognosis and therapy response in colorectal cancer. *Nat Med.* January  
602 9, 2023; Available at: <http://dx.doi.org/10.1038/s41591-022-02134-1>
- 603 28. Loupakis F, Sharma S, Derouazi M, Murgioni S, Biondi P, Rizzato MD, et al. Detection of  
604 Molecular Residual Disease Using Personalized Circulating Tumor DNA Assay in Patients With  
605 Colorectal Cancer Undergoing Resection of Metastases. *JCO Precis Oncol.* July 2021;5.  
606 Available at: <http://dx.doi.org/10.1200/PO.21.00101>
- 607 29. Macenko M, Niethammer M, Marron JS, Borland D, Woosley JT, Guan X, et al. A method for  
608 normalizing histology slides for quantitative analysis. In 2009 IEEE International Symposium on  
609 Biomedical Imaging: From Nano to Macro 2009; 1107–1110.
- 610 30. Chen RJ, Ding T, Lu MY, Williamson DFK, Jaume G, Song AH, et al. Towards a general-purpose  
611 foundation model for computational pathology. *Nat Med.* March 2024;30(3):850–862.

- 612 31. Katzman JL, Shaham U, Cloninger A, Bates J, Jiang T, Kluger Y. DeepSurv: personalized  
613 treatment recommender system using a Cox proportional hazards deep neural network. *BMC*  
614 *Med Res Methodol*. February 26, 2018;18(1):24.
- 615 32. Ueno H, Ishiguro M, Nakatani E, Ishikawa T, Uetake H, Murotani K, et al. Prognostic value of  
616 desmoplastic reaction characterisation in stage II colon cancer: prospective validation in a Phase  
617 3 study (SACURA Trial). *Br J Cancer*. March 2021;124(6):1088–1097.
- 618 33. Lugli A, Karamitopoulou E, Zlobec I. Tumour budding: a promising parameter in colorectal  
619 cancer. *Br J Cancer*. May 22, 2012;106(11):1713–1717.
- 620 34. Platten M, Bunse L, Wick A, Bunse T, Le Cornet L, Harting I, et al. A vaccine targeting mutant  
621 IDH1 in newly diagnosed glioma. *Nature*. April 2021;592(7854):463–468.
- 622 35. Huijbers A, Tollenaar RAEM, Pelt GW v, Zeestraten ECM, Dutton S, McConkey CC, et al. The  
623 proportion of tumor-stroma as a strong prognosticator for stage II and III colon cancer patients:  
624 validation in the VICTOR trial. *Ann Oncol*. January 2013;24(1):179–185.
- 625 36. Hu Q, Wang Y, Yao S, Mao Y, Liu L, Li Z, et al. Desmoplastic Reaction Associates with  
626 Prognosis and Adjuvant Chemotherapy Response in Colorectal Cancer: A Multicenter  
627 Retrospective Study. *Cancer Research Communications*. June 15, 2023;3(6):1057–1066.
- 628 37. Wulczyn E, Steiner DF, Moran M, Plass M, Reihls R, Tan F, et al. Interpretable survival prediction  
629 for colorectal cancer using deep learning. *NPJ Digit Med*. April 19, 2021;4(1):71.
- 630 38. Grothey Axel, Sobrero Alberto F., Shields Anthony F., Yoshino Takayuki, Paul James, Taieb  
631 Julien, et al. Duration of Adjuvant Chemotherapy for Stage III Colon Cancer. *N Engl J Med*.  
632 March 29, 2018;378(13):1177–1188.
- 633 39. Zaborowski AM, Winter DC, Lynch L. The therapeutic and prognostic implications of  
634 immunobiology in colorectal cancer: a review. *Br J Cancer*. November 2021;125(10):1341–1349.
- 635 40. Sun C, Li B, Wei G, Qiu W, Li D, Li X, et al. Deep learning with whole slide images can improve  
636 the prognostic risk stratification with stage III colorectal cancer. *Comput Methods Programs*  
637 *Biomed*. June 2022;221:106914.